Received: 18 May 2021 | Revised: 2 July 2021 | Accepted: 28 July 2021

DOI: 10.1111/ijag.16505

INTERNATIONAL JOURNAL OF Applied Glass SCIENCE

RESEARCH ARTICLE

Niobate in silicate and phosphate glasses: Effect of glass basicity on crucible dissolution

Natalia A. Wójcik[1,2,3] | **Sharafat Ali**[3] | **Efstratios I. Kamitsos**[4] | **Doris Möncke**[3,4,5]

[1]Advanced Materials Center, Gdańsk University of Technology, Gdańsk, Poland

[2]Institute of Nanotechnology and Materials Engineering, Faculty of Applied Physics and Mathematics, Gdańsk University of Technology, Gdańsk, Poland

[3]Department of Built Environment and Energy Technology, Linnaeus University, Växjö, Sweden

[4]Theoretical and Physical Chemistry Institute, National Hellenic Research Foundation, Athens, Greece

[5]Inamori School of Engineering at the New York State College of Ceramics, Alfred University, Alfred, New York, USA

Correspondence
Natalia A. Wójcik, Advanced Materials Center, Gdańsk University of Technology, ul. Narutowicza 11/12, 80-233 Gdańsk, Poland.
Email: natalia.wojcik@pg.edu.pl

Funding information
ARGENTUM TRIGGERING RESEARCH GRANTS - 'Excellence Initiative - Research University', Grant/Award Number: DEC-19/2020/IDUB/I.3.3; VINNOVA, Grant/Award Number: 2015-04809; Stiftelsen för Kunskaps- och Kompetensutveckling, Grant/Award Number: 68110029; Crafoord Foundation, Grant/Award Number: 20160900; European Union, Grant/Award Number: MIS 5002409

Abstract

Using niobium crucibles for melting phosphate and silicate glasses of various modifier oxide contents, and therefore varying optical basicity (Λ), was found to result in varying dissolution rates of niobate during melting. Because of their high electronic polarizability, even small concentrations of niobates are detectable in the Raman spectra of glasses. Even <1 mol% Nb_2O_5 can be identified, as independently confirmed by SEM-EDX analysis. Silica-rich glasses (~60% SiO_2, Λ ~0.6) did not show significant Nb dissolution from the crucible, while higher basicity metasilicate glasses (~50% SiO_2, Λ ~0.65) and pyrophosphate glasses (~30% P_2O_5, Λ ~0.7) did show the typical niobate signature in the Raman spectra at 810–840 cm^{-1}, depending on composition. While niobium is well-dissolved throughout the pyrophosphate glass, metasilicate glasses showed a much more intense Raman signature of niobate units near the outer surface of the glass. Measurements along the cross-section of a fractured metasilicate glass showed a steady decrease of the strength of the niobate signature from the surface toward the bulk of the material. Besides correlation with optical basicity, the tendency of melts to dissolve Nb crucible was discussed in terms of the connectivity or polymerization of the network and the corresponding melt viscosity.

KEYWORDS

crucible dissolution, Niobate in glasses, optical basicity, phosphate and silicate glasses, Raman spectroscopy

1 | INTRODUCTION

In recent years, the effect of the crucible material on glass composition, structure and, subsequently, the glass thermal, electrical and mechanical properties has attracted increasing attention in glass chemistry and physics.[1–7] Especially, the dissolution of alumina crucibles was shown to modify phosphate, silicate, or tellurite networks through addition of Al_2O_3 leached from the crucible. Differences in the glass transition temperature T_g by as much as 100°C have been observed, while the glass network is substantially altered and, especially for tellurium dioxide, glass formation is significantly enhanced.[1,5] Melting phosphate glasses in silica crucibles is also known to dissolve silicate species into the glass, though dissolution seems to be less when compared to alumina crucibles.[8] Dissolution of traces of Pt metal particles can be problematic in the preparation of phosphate-based laser glasses,[9] not to mention the complex and harmful interaction of reduced elements with platinum, which is especially challenging for phosphate glasses.[10]

Usually, melting oxide glasses in research laboratories is performed, under air using the conventional melting technique. This involves mixing oxide precursors, often supported by ball milling, melting of the mixture in an alumina or platinum crucible for certain time and, at the end, fast quenching to room temperature. Methods different than the conventional are also employed for the preparation of glasses including the sol-gel technique,[11] melting in a reducing atmosphere,[12–15] and twin roller very fast-cooling.[16] Sometimes, a two-step synthesis route is used as, for example, when incorporating nitrogen into silicate glass networks (e.g. through the addition of Si_3N_4[13,17–20] or into phosphate glasses.[12] In the first step of this technique, the parent glass is melted in alumina or platinum crucibles. In the second step, the glass is re-melted with the addition of powdered Mg/Ca metal or Si_3N_4 in suitable crucibles and under reducing atmosphere with inductive heating. Metallic niobium (Nb) crucibles are used in inductive heated furnaces, as is metallic tungsten (W) and molybdenum (Mo) crucibles. Significant literature is available on the use of Mo-electrodes in glass melts and their corrosion by the melts.[21,22] In small laboratory scale melts, no niobate-dissolution had been observed earlier for silicate glasses prepared under conditions comparable to those described in the current study.[18,19] However, we have shown that phosphate glasses can dissolve niobate from the crucible material during melting.[12]

In this work, we have studied systematically and discussed the effect of melting three different series of phosphorous-silicate glasses in niobium crucibles with regard to the dissolution of crucible material and its effect on the glass structure. Emphasis was placed on glass basicity and its role on niobate dissolution from the crucible, by considering glasses close to metasilicate (~50 mol% SiO_2) and pyrophosphate (~30 mol% P_2O_5) compositions as well as glasses with high SiO_2 content (~60 mol% SiO_2). The first two series of investigated glassy materials were prepared using a two-step synthesis route, which is only briefly summarized here since it was described elsewhere in more detail.[12–14] The last series was directly melted in niobium crucibles. Niobium dissolution was analyzed by scanning electron microscopy (SEM) and its effect on glass structure was studied by Raman spectroscopy, the latter technique was also used to highlight differences in the distribution of niobium in various oxide melts.

2 | EXPERIMENTAL PROCEDURE

2.1 | Glass preparation

Three different glass series were synthesized and compared: Series I, phosphate doped-meta-silicate glasses Mg/Ca–Na_2O–CaO–P_2O_5–SiO_2 (~50 mol% SiO_2 and up to 5 mol% P_2O_5); Series II, phosphate rich glasses Mg–Na_2O–CaO–SiO_2–P_2O_5–P_3N_5 close to the pyrophosphate composition (~30 mol% P_2O_5); and Series III, Na_2O/Li_2O–BeO–SiO_2–Si_3N_4 glasses with high SiO_2 content (~60 mol% SiO_2). Samples of series I and II were prepared using the two step synthesis route and details of the used parameters are listed in Table 1, while the analyzed glass compositions are listed in Table 2 (see previous reports for synthesis details[12–14]). In excess to the nominal composition, Al and niobate were found in the as-prepared glasses. Silicate glasses of series III doped with BeO were prepared directly in niobium crucibles, without a preliminary melting step as used for the phosphate containing glasses which were premelted in Al_2O_3 crucibles. This is due to the fact that BeO reacts easily with Al_2O_3, and high contents of the latter might otherwise be incorporated into the glass.[23] No significant niobate impurities were found in beryllium-doped glass samples (Table 2). BeO is a hazardous compound and, thus, it requires working under a fume hood throughout preparation and melting. We advise to consult local safety regulation when reproducing the present melting experiments.

The used niobium crucibles were cone shaped. They had an outside diameter of 10 mm, wall thickness 0.4 mm, and height of 20 mm and were prepared from niobium of purity 99.9%. Due to the vertical construction of tube furnace, the glass could only be recovered by breaking the crucible after melting, but the crucible separated easily from the glass.

TABLE 1 Summary of sample preparation parameters for Series I, II, and III materials, with T_m (melting temperature), t_m (melting time), atm (melting atmosphere), CM (crucible material), furnace for melting with IF induction furnace and MF muffle furnace

Samples	Starting composition (mol%)	T_m (K)	t_m (min)	atm	CM	Mean batch mass (g)	Furnace for melting	Cooling
Series I: P doped metasilicate glasses Mg/Ca–Na_2O–CaO–P_2O_5–SiO_2								
Target glass	$25Na_2O$–20CaO–$5P_2O_5$–$50SiO_2$	1623	30	Air	Al_2O_3	26	MF	Quenched to cold water
Series doped with Mg – SixMg where x is 1, 2, 3, 4, 5	xMg–(100-x)($25Na_2O$–20CaO–$5P_2O_5$–$50SiO_2$)	1773–1823	60	N_2	Nb	1	IF	Cooling in the furnace to RT for 1 h
Series doped with Ca – SixCa where x is 1, 2, 3, 4, 5	xCa–(100-x)($25Na_2O$–20CaO–$5P_2O_5$–$50SiO_2$)	1823–1923	60	N_2	Nb	1	IF	Cooling in the furnace to RT for 1 h
Series II: P rich glasses Mg–Na_2O–CaO–SiO_2–P_2O_5–P_3N_5								
1st target glass	$40Na_2O$–20CaO–$40P_2O_5$	1273	30	Air	Al_2O_3	10	MF	Quenched to cold water
Series doped with Si_3N_4 and Mg P5, P6 P7	$x$$Si_3N_4$–1Mg–(99-$x$) ($40Na_2O$–20CaO–$40P_2O_5$)	1373–1773	60–120	N_2	Nb	1	IF	Cooling in the furnace to RT for 1 h
2nd target glass	1Si_3N_4–99($40Na_2O$–20CaO–$40P_2O_5$)	1273–1373	30	Air	Al_2O_3	10		Quenched to cold water
Series doped with Mg P8, P9, P10, P11	xMg–(100-x)[1Si_3N_4–99($40Na_2O$–20CaO–$40P_2O_5$)]	1673–1873	60–120	N_2	Nb	1	IF	Cooling in the furnace to RT for 1 h
Series III: BeO-silicate glasses Na_2O/Li_2O–BeO–SiO_2–Si_3N_4								
Series doped with Na_2O SixNNa where x is 1, 2, 3, 4, 5	$35Na_2O$–5BeO–(60-x) SiO_2–$x$$Si_3N_4$	1723–1823	60	N_2	Nb	1.5	IF	Cooling in the furnace to RT for 1 h
Series doped with Na_2O and Li_2O SixNLiNa where x is 1, 2, 3, 4, 5	$9Li_2O$–$27Na_2O$–5BeO–(59-x)SiO_2–$x$$Si_3N_4$	1723–1873	60–120	N_2	Nb	1.5	IF	Cooling in the furnace to RT for 1 h

2.2 | EDS measurements

The final composition of a glass melted using the two-step synthesis procedure may deviate from the original composition due to Al and/or Nb incorporation from the crucibles, as well as the target nitride incorporation when melting under a nitrogen atmosphere. Therefore, the real compositions of all glasses were determined with the use of energy dispersive spectroscopy (EDS) technique on the fractured samples. Series I, P-doped meta-silicate[14] and Series II, phosphate rich[12] samples were tested using a high-resolution scanning electron microscope, SEM (LYRA3, TESCAN) equipped with EDS detector (EDAX). Series III, oxynitride silicate glasses[13] were investigated using a SEM (FEI Company Quanta FEG250), with Energy Dispersive X-ray Spectrometer (EDAX GENESIS Apex Apollo X60), as well as using an inductively coupled plasma optical emission spectrometer (ICP-OES, Hitachi High-Technologies Corp., Model SPS3520UV-DD) and a nitrogen and oxygen elemental analyzer (LECO Corp., TC-436AR).

TABLE 2 Glass IDs and analyzed glass composition in mol% for all samples in Series I, II and III

Series I: Phosphorous-silicate glasses Mg/Ca–Na_2O–CaO–P_2O_5–SiO_2[14]										
Glass ID	**Si1Mg**	**Si2Mg**	**Si3Mg**	**Si4Mg**	**Si5Mg**	**Si1Ca**	**Si2Ca**	**Si3Ca**	**Si4Ca**	**Si5Ca**
Na_2O	25.9	25.5	25	23.5	24	28.2	25.8	26.3	24.9	24.4
CaO	21.0	19.9	20	19.7	20.3	18.2	20.2	21.3	21.9	22.8
MgO	1.5	2.1	2.4	2.7	3.6	0	0	0	0	0
Al_2O_3	0.4	0.3	0.4	0.6	0.7	0.3	0.3	0.3	0.3	0.3
SiO_2	45.9	48.4	48.9	48.9	46.3	49.5	49.6	47.6	48.2	47.6
P_2O_5	5.1	3.7	3.6	4.3	4.6	3.6	4	4.3	4.6	4.7
[b]Nb_2O_5	0.1	0.1	0.1	0.3	0.4	0.1	0.1	0.1	0.1	0.1

Series II: Phosphate glasses Mg–Na_2O–CaO–SiO_2–P_2O_5–P_3N_5[12]							
ID	**P5**	**P6[a]**	**P7[a]**	**P8**	**P9[a]**	**P10[a]**	**P11[a]**
Na_2O	43.5	42.5	39.4	43.0	41.4	30.2	30.7
CaO	20.4	20.1	19.7	19.3	19.1	27.6	26.5
MgO	1.2	1.4	1.5	2.9	3.7	4.4	5.3
Al_2O_3	0.4	0.2	0.3	0.5	0.3	6.2	7.0
SiO_2	2.5	6.9	8.5	3.1	3.1	5.3	3.7
P_2O_5	28.9	22.2	27.7	29.4	30.3	27.6	26.5
P_3N_5	1.6	4.0	1.8	1.1	1.2	3.1	2.4
[b]Nb_2O_5	1.5	2.7	1.0	0.6	0.9	3.0	3.0

Series III: Oxynitride silicate glasses Na_2O/Li_2O–BeO–SiO_2–Si_3N_4[13]										
ID	**Si1NNa**	**Si2NNa**	**Si3NNa**	**Si4NNa**	**Si5NNa**	**Si1NLiNa**	**Si2NLiNa**	**Si3NLiNa**	**Si4NLiNa**	**Si5NLiNa**
Na_2O	34.2	33.4	33	33.7	33.3	24.5	24.5	25.1	25.3	25.4
Li_2O	0	0	0	0	0	9.9	10.0	9.9	10.1	10.1
BeO	5.2	5.2	4.9	5.2	5.0	5.2	5.2	5.2	5.2	5.4
SiO_2	60.0	60.4	60.6	59.0	59.4	59.8	59.3	58.3	57.3	56.7
Al_2O_3	0	0	0	0	0	0	0	0	0	0
Si_3N_4	0.7	1.0	1.5	2.2	2.2	0.7	1.1	1.4	2.1	2.4
[b]Nb_2O_5	0	0	0	0	0	0	0	0	0	0

[a]Devitrified glass.

[b]As measured by SEM-EDS on the bulk sample, if present, Nb was below the detection limit.

2.3 | Raman spectroscopy

The structure of the synthesized glasses and the Nb_2O_5 incorporation was studied by Raman spectroscopy. Raman measurements were performed in the range from 100 to 2000 cm^{-1} with a resolution of 2 cm^{-1} on a dispersive confocal Raman microscope (Renishaw inVia), using the 488, 514.5, or 633 nm laser excitation lines. The use of different excitation lines was dictated by the fluorescence of some samples.

For the P-doped meta-silicate type glasses (Series I), the measurements conducted on fresh cross-sections and on the outer surfaces of the glass samples showed such a big difference in the Nb signal, that additional Raman measurements were performed at 11 points on a cross-section from the surface of the sample toward the bulk (glass Si3Ca, see Table 2 for details). This line measurement, covering a range of ca. 1365 μm, was carried out in order to examine the sample homogeneity or gradual variations in the niobate content. The Raman cross-section distances are based on readings of the variations of the x value for near constant y and z coordinates when moving the stage with the sample. For focusing and aiming at a flat spot on the broken sample's surface, y and z were minimally adjusted. The (x,y,z) coordinates of the start point (0,0,0) and end point are shown in the sketch (Figure 1). The final point was measured on the samples surface after rotating the sample (red arrow). The same measurements have not been taken on the other samples. Spectra have been normalized on the strongest Raman band intensity

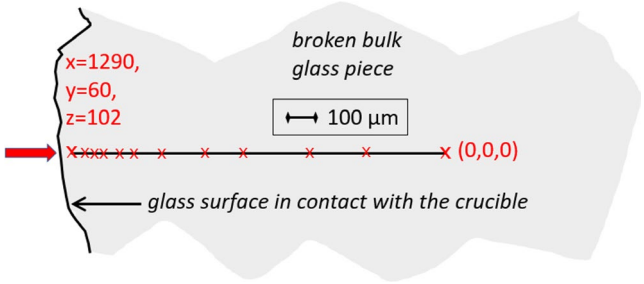

FIGURE 1 Sketch of Si3Ca sample cross-section with the points of Raman spectroscopy measurements

in the range of 200–1400 cm^{-1} and offset for clarity. The estimated error in the Raman band position is ±1 cm^{-1}.

3 | RESULTS AND DISCUSSION

3.1 | Glass composition

Table 2 presents the analyzed glass composition for Series I phosphorous-silicate glasses; SixMg and SixCa from Ref. [14], selected samples from Series II phosphate glasses (Px) reported in Ref. [12] and Series III oxynitride silicate glasses (SixNNa and SixNLiNa) described in Ref. [13], with the sample names being taken from the cited references to facilitate comparison of the current paper with our earlier publications. For Series I and Series II glasses the quantitative analysis by SEM-EDS showed a significant niobium content resulted from the dissolution of the Nb crucibles (expressed as Nb_2O_5 in Table 2). The silicate rich glasses (Series III) showed no niobate impurities (below the limit of SEM-EDS) after melting under nitrogen, while N-incorporation was much more successful.

3.2 | Optical basicity

We expect that niobium solubility might be enhanced in glasses with higher optical basicity, which describes the electron donor power of the glass matrix and provides a very successful parameter when comparing different glass systems.[24] This is especially important when these systems might not show any common systematic compositional variations, such as the three glass series considered in this study.

Accordingly to Duffy and Ingram, the optical basicity, Λ, calculated on the basis of the glass composition[25,26] is a very helpful parameter for comparing acid-base properties of glasses, redox equilibria or optical properties such as refractive index and band gap. In oxide glasses, a high value of this parameter correlates with a high fraction of modifier metal oxides, which are generally characterized by higher polarizabilities than conventional network former oxides. Subsequently, a depolymerized glass network with many nonbridging oxygen atoms and ionic bonds would have higher basicity than a more polymerized network with covalent bridging bonds between oxygen and network of former atoms such as B, P, or Si, the latter having very low polarizabilities.

The theoretical optical basicity for any oxide glass of composition $aA_xO_y - bB_pO_q$ - ... can be evaluated with the use of the Duffy and Ingram relation[25,26]:

$$\Lambda_{th} = \frac{X_A}{\gamma_A} + \frac{X_B}{\gamma_B} + \cdots = \frac{ya}{ya+qb+\cdots}\Lambda\left(A_xO_y\right) + \frac{qb}{ya+qb+\cdots}\Lambda\left(B_pO_q\right) + \cdots, \quad (1)$$

where $1/\gamma_A = \Lambda(A_xO_y)$... is the optical basicity of oxide A_xO_y, etc. Values of Λ have been tabulated by various research groups and are constantly expanded to oxides of other elements, as well as refined and updated.[26–28] The oxide basicities are weighted by the oxygen equivalent fractions X_A, etc. The values of optical basicity of silicate SixMg and SixCa glasses (Series I) were calculated according to relation (1), using the optical basicity values of the various oxides given in Refs [25,28] ($\Lambda(Na_2O) = 1.105$, $\Lambda(CaO) = 1.0$, $\Lambda(P_2O_5) = 0.48$, $\Lambda(MgO) = 0.78$, $\Lambda(Al_2O_3) = 0.61$, $\Lambda(SiO_2) = 0.48$), while the value of optical basicity $\Lambda(Nb_2O_5) = 1.05$ was taken from Ref. [29]

To calculate the optical basicity of oxynitride phosphate Px (Series II) and silicate SixNNa and SixNLiNa (Series III) glasses, we applied the newest findings from Ref. [30] where the optical basicity of nitride compounds was related to the corresponding oxide basicity by $\Lambda(M_3N_m) = 3/2\ \Lambda(M_2O_m)$. To simplify the calculation, it was assumed that all nitrogen detected in silicate SixNNa and SixNLiNa glasses is present in the Si_3N_4 form and as P_3N_5 in Px samples. The values used for the optical basicities of Si_3N_4 and P_3N_5 are therefore $\Lambda(Si_3N_4) = \Lambda(P_3N_5) = 0.72$. Moreover, we used the values $\Lambda(BeO) = 0.375$ and $\Lambda(LiO_2) = 0.81$ from Refs [29, 26] respectively.

The calculated basicity values Λ_{th} of glasses, using their analyzed compositions in Table 2 and Equation (1), are listed in Table 3. The lowest values of optical basicity were found for the oxynitride silicate glasses with ~60 mol% SiO_2 content (Series III) with Λ_{th} between 0.595 and 0.617. These values are close to those obtained for the $1Na_2O{:}2SiO_2$ disilicate glass.[26] For comparison, phosphorous-silicate glasses of Series I containing no highly polarizable nitrogen anions but higher quantities of modifier oxides (~50 mol% SiO_2), exhibit optical basicity values between 0.639 and 0.649. The highest values of optical basicity are found for the pyrophosphate glasses and devitrified glasses of Series II which contain also the

TABLE 3 Optical basicity values Λ_{th} calculated according to Equation 1 and the analyzed sample compositions in Table 2

Series I: Phosphorous-silicate glasses Mg/Ca–Na_2O–CaO–P_2O_5–SiO_2										
ID	**Si1Mg**	**Si2Mg**	**Si3Mg**	**Si4Mg**	**Si5Mg**	**Si1Ca**	**Si2Ca**	**Si3Ca**	**Si4Ca**	**Si5Ca**
Λ_{th}	0.648	0.647	0.647	0.639	0.648	0.647	0.643	0.649	0.644	0.645
Series II: Phosphate glasses Mg–Na_2O–CaO–SiO_2–P_2O_5–P_3N_5										
ID	**P5**		**P6**		**P7**		**P8**		**P9**	**P10**	**P11**
Λ_{th}	0.673		0.704		0.655		0.660		0.655	0.701	0.700
Series III: Oxynitride silicate glasses Na_2O/Li_2O–BeO–SiO_2–Si_3N_4										
ID	**Si1NNa**	**Si2NNa**	**Si3NNa**	**Si4NNa**	**Si5NNa**	**Si1NLiNa**	**Si2NLiNa**	**Si3NLiNa**	**Si4NLiNa**	**Si5NLiNa**
Λ_{th}	0.612	0.610	0.611	0.617	0.615	0.595	0.597	0.602	0.606	0.608

highest amount of modifier oxides (~30 mol% P_2O_5); with Λ_{th} between 0.655 and 0.704.

Increased glass basicity is expected with the addition of alkali and alkaline earth oxides, since these are more polarizable than the network former oxides. Despite the very low basicity of BeO, this trend is also observed for all samples of the current study, as it is apparent from the trend in optical basicity versus total modifier oxide content shown in Figure S1a. The Figure S1b presents the optical basicity behavior for SixMg, SixCa, SixNNa, and SixNLiNa glasses in a higher magnification. The optical basicity is found for all silicate glasses to increase approximately linearly with total modifier content, while pyrophosphate glasses appear to partially deviate from this trend. It is noted that the higher concentrations of Nb_2O_5 and nitrides in the phosphate glasses of Series II significantly increase the optical basicity of these glasses. Interestingly, the three phosphate devitrified glasses which exhibit the highest values of optical basicity (e.g. P6, P10, P11) in Figure S1a contain the highest quantity of Nb_2O_5 and nitrogen among all samples.

Figure 2 shows the correlation between optical basicity and niobate solubility. While Nb_2O_5 has a higher oxide polarizability and consequently a higher contribution to optical basicity than the network former oxides, and even most alkali and alkali earth oxides, the dissolved fraction is small and not the driver of the high basicity. Calculating the optical basicity for presumed niobate-free samples of otherwise analogues modifier to former compositions, does show the same trend, i.e. the highest basicity for those glasses that ultimately dissolve the most niobium. Figure S2 displays the influence of nitrogen content on the optical basicity for Px, SixNNa, and SixNLiNa samples. A clear increase in the values of Λ_{th} with the increase in nitride compound concentration is found for each of the two series. These glasses have a overall low optical basicity, highly polymerized networks and do not dissolve significant amounts of niobate species. The higher polarizability

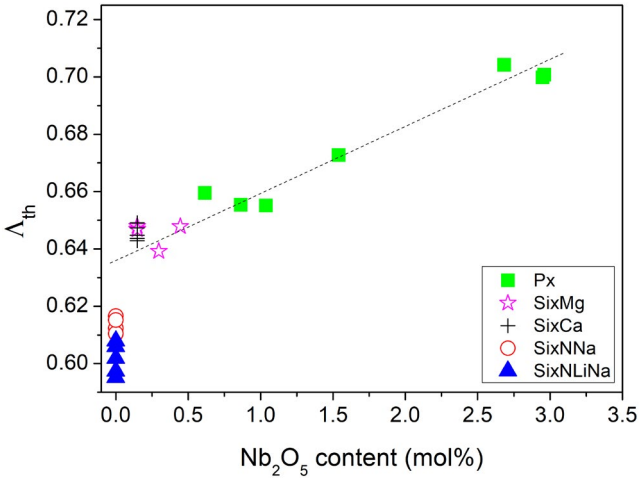

FIGURE 2 Optical basicity correlation with the Nb_2O_5 content for all samples in Series I, II, and III. Straight line is only a guide for eyes

of nitrogen versus oxygen might drive some of the observed basicity increase.

3.3 | Glass structure by Raman spectroscopy

3.3.1 | The structure P-doped meta silicate glasses (50 mol% SiO_2)

First, we start with a brief discussion of the Raman spectra of SixMg and SixCa glasses (Series I), which were not considered in previous reports. The Raman spectra for selected glasses from the Mg-series and Ca-series are shown in Figure 3A,B, respectively, as obtained on fresh cross-sections (bulk) with laser excitation at 488 nm. All samples show similar sets of only a handful of relatively broad bands as marked on the figure, which are typical for amorphous materials. Raman assignments are

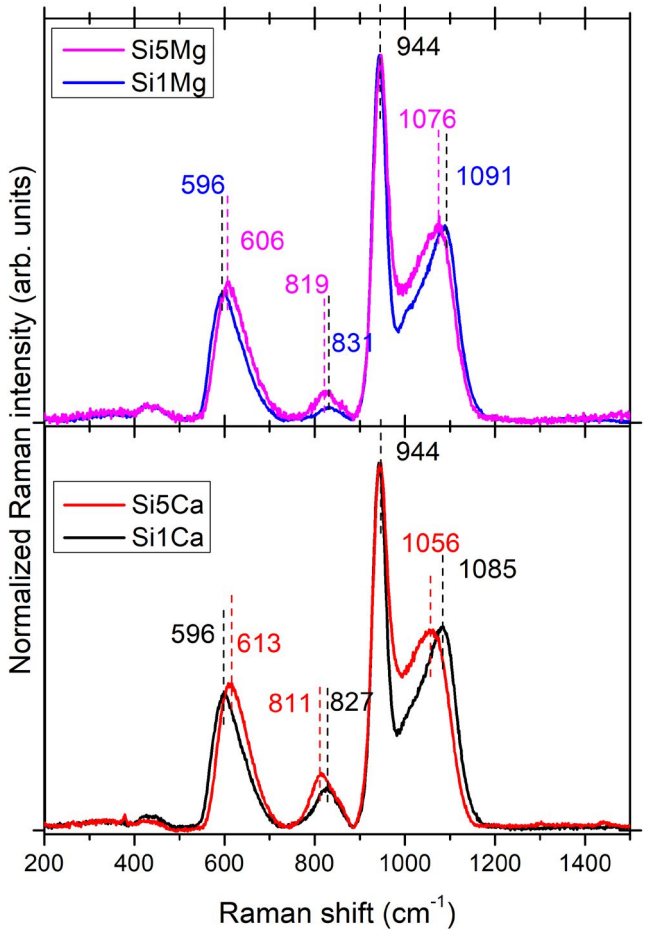

FIGURE 3 Raman spectra for (A) Mg-glasses (top) and (B) Ca-glasses (bottom). Raman spectra were obtained from the interior of fractured bulk samples using the 488 nm laser line for excitation. Spectra are normalized to the highest intensity peak at 944 cm^{-1}. Bands positions are indicated for samples in each figure

based on the detailed works of Furukawa et al.[31] and others.[32–40]

The Raman spectra of the Si1Mg and Si1Ca glasses exhibit the strongest Raman band at 944 cm^{-1}, while weaker bands are seen around 1085 and 596 cm^{-1}. According to literature,[32–42] the highest intensity band at 944 cm^{-1} is due to the symmetric stretching vibration of silicate SiO_4 tetrahedral units with two bridging and two nonbridging oxygen atoms, $\nu(Q^2)$, where the superscript in Q^2 denotes the number of bridging oxygen atoms. The higher-frequency band at 1085 cm^{-1} has been attributed to the analogous symmetric stretching of silicate tetrahedra with three bridging and one nonbridging oxygen atoms, $\nu(Q^3)$. The band at 596 cm^{-1} is due to intertetrahedra Si–O–Si stretching-bending vibration in these depolymerized structural units, ν(Si–O–Si).

Systematic changes are observed in the Raman spectra of the SixMg and SixCa glasses compared to the corresponding spectra of the least modified Si1Mg and Si1Ca glasses. First, the ν(Si–O–Si) frequency at 596 cm^{-1} increases with increasing Mg and Ca levels to ~606 (5Mg) and to 613 cm^{-1} (5Ca), as presented in Figure 3. Second, the high-frequency Raman band, $\nu(Q^3)$, downshifts from ~1091 cm^{-1} (1Mg) to 1076 cm^{-1} (5Mg) and from ~1085 cm^{-1} (1Ca) to 1056 cm^{-1} (5Ca). These changes suggest the decrease in the polymerization of the silicate network, i.e. the increase in the relative population of Q^2 groups. Similarly, Furukawa et al. observed upshift of the ca. 600 cm^{-1} band and downshift of the ca. 1070 cm^{-1} band with increasing network depolymerization in Na_2O–SiO_2 glasses.[31]

Figure 3 shows that the Q^3 peak at 1085–1090 cm^{-1} exhibits a distinct asymmetry at its low-frequency side. According to the literature, multiple bands are required to describe the high-frequency region of the Raman spectra of silicate glasses where silicon-oxygen stretching vibrations of Q^n units are active.[31,43–46] Therefore, the asymmetry of the Q^3 peak indicates the presence of Q^3 units with different bonding environments which may result from different connectivities with other Q^3 and Q^2 units, or from different charge balancing modifier cations. For example, Velli et al. found a significant shift in the Raman position upon variation of the field strength of the modifier cation in metaphosphate glasses.[47]

All glasses in the SixMg and SixCa series exhibit an additional band at ~810–830 cm^{-1} depending on glass composition. Also, the intensity of this band relative to the silicate bands appears to change with distance of the probed spot from the glass surface (see Figure 4). A similar band at about 890 cm^{-1} was observed in phosphate glasses that had been re-melted in niobium crucibles and was assigned to stretching vibrations of Nb–O bonds of NbO_6 octahedral groups.[48–51] As indicated by Figure 3, the niobate band at 810–830 cm^{-1} gains relative intensity upon increasing depolymerization of the silicate network. The relation of this band with the dissolved niobium from the crucible will be discussed in the following section.

3.3.2 | Niobate levels in glass by Raman and SEM techniques

The high polarizability of Nb ions, $\alpha(Nb^{5+}) = 0.242$ Å^3, compared to the low polarizability of Si ions, $\alpha(Si^{4+}) = 0.033$ Å^3,[52] results in an exceptional high scattering cross-section for niobate-related vibrational bands. Subsequently, even traces of dissolved niobates (0.1 at.% of Nb) can be identified by Raman spectroscopy. As mentioned above, the intensity of the 810–830 cm^{-1} band is relatively weak in the bulk of glass but increases as the probed volume approaches the samples interface with the niobium crucible. This is demonstrated in Figure 4 on a ca. 1365 μm long

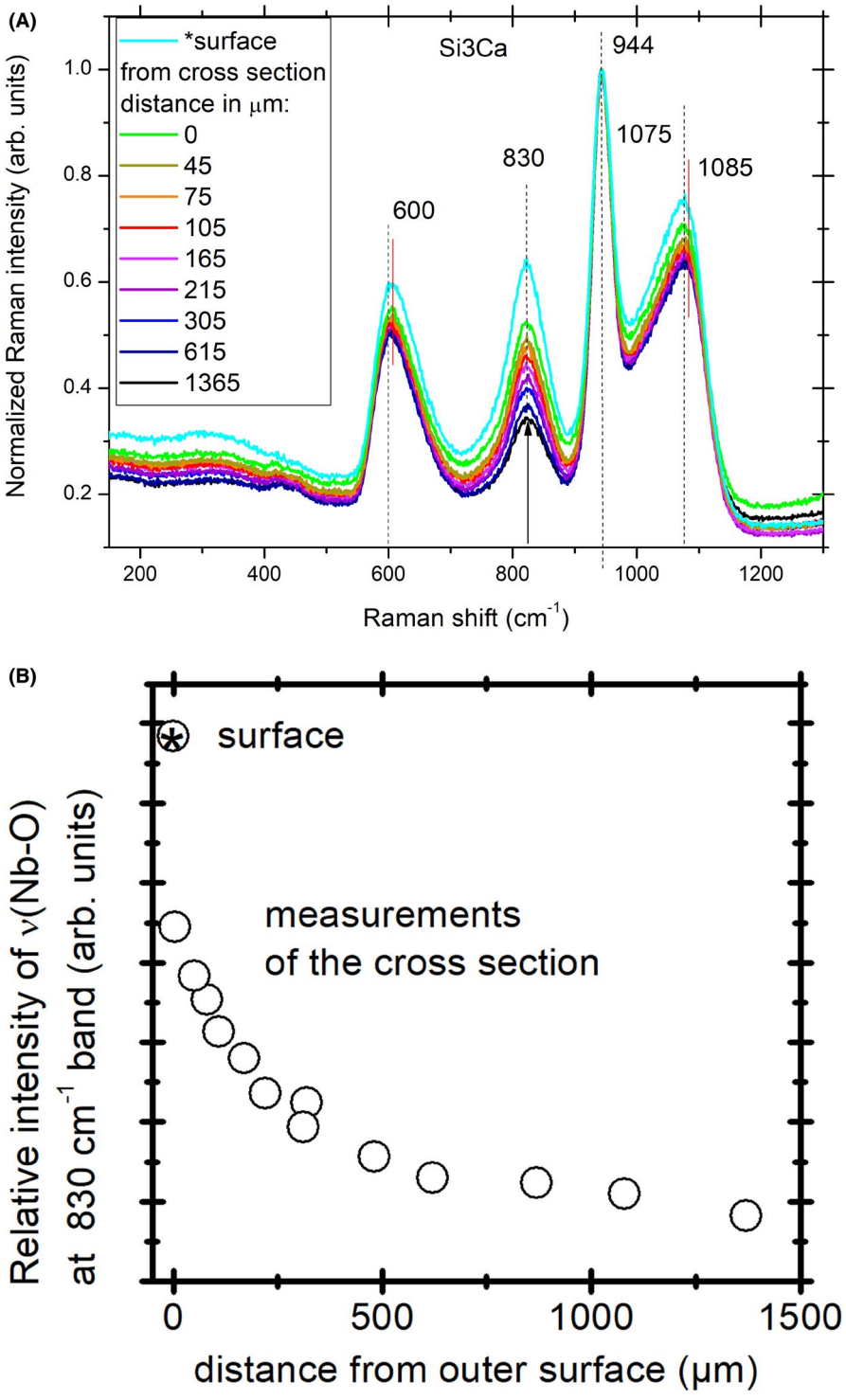

FIGURE 4 (A) Raman spectra for glass Si3Ca measured with the 488 nm excitation line and normalized on the highest intensity Q^2 peak at 944 cm^{-1}. The spectra were collected directly from the surface (marked with *) and from a broken cross section on spots along a line from the outer surface toward the bulk by moving the laser spot with increasing step sizes (see Figure 1). Vertical dashed lines in (A) are drawn to indicate band positions around 600, 830, and 1075 cm^{-1}. Spectra have been offset to allow comparison. (B) shows the relative intensity of ν(Nb–O) band at 830 cm^{-1} as a function of distance from outer surface estimated from (A)

line on the cross section of sample Si3Ca, scanning from the glass surface to inner material. The highest intensity of the niobate band at 830 cm^{-1} is observed for measurements obtained from the sample surface, which was in contact with the niobate-crucible during melting and cooling. This is also consistent with the parallel increasing intensity at about 300 cm^{-1}, where contributions from bending vibrations of niobate species are expected. Thus, the presence of niobates in the glass is a consequence of the synthesis route employed, i.e. having the melt in contact with the niobium crucible. Similarly, low levels of niobate were found dissolved into the bulk of phosphate glasses, as probed from the broken samples' interior.[12]

Comparison of the analyzed niobate content found in the bulk material by SEM-EDS, which was measured to be ~0.1 at.% (Table 2), with the intensity changes of the Raman band at about 830 cm^{-1} relative to the strong Q^2 silicate signal at 944 cm^{-1} suggests that the niobate

content in the surface layer is approximately ~0.25 at.%, which is more than two times higher than in the bulk sample. Interesting are also the consequent effects on the silicate bands at ca. 600 cm^{-1}, ν(Si–O–Si), and 1085 cm^{-1}, $\nu(Q^3)$. The first band slightly upshifts and the second downshifts with increasing niobate-dissolution from the bulk to the surface, indicating the progressive depolymerization of the silicate network in the same direction.

The change in niobate content from the bulk to the glass surface might be due to a combination of several melting processing and other parameters, such as solubility, basicity, melt viscosity, and diffusivity. An increased degree of cross-linking of silicate tetrahedra through Nb^{5+} ions would certainly increase the melt viscosity and, thus, impede the ease of homogenization in this stirrer-free melt. Also, the melting temperature and time as well as the cooling time in the niobium crucible should affect the amount of the dissolved niobate. The cooling time was approximately 1 h that is rather long compared to the melting process of glass.

As mentioned earlier, niobium dissolution has been discussed for phosphate glasses but not for oxynitride-silicate glasses. Therefore, we probed bulk and surface areas of a series of oxynitride-silicate glasses for signs of the characteristic niobate Raman signature. Typical results are displayed in Figure 5 for the Si1NNa glass, while the detailed description of the structure was presented in Ref. [13]. This glass is clearly more polymerized compared to that of Figure 4 as its main band is measured at about 1090 cm^{-1} and reflects the stretching of $Si–O^-$ bonds in Q^3 units. In addition, the corresponding Q^2 band at about 950 cm^{-1} is considerably weaker than that of sample Si3Ca (Figure 4). Important in the context of the current study is the strong signal at 840 cm^{-1} measured on the glasses surface of Si1NNa that was in contact with the crucible material; this signal is completely absent from the bulk of the sample as probed on a freshly broken glass surface. This result is in contrast with that of sample Si3Ca, whose bulk shows the presence of the 840 cm^{-1} band (Figure 4). This comparison shows that oxynitride-silicate melts (Series III) with relatively polymerized silicate networks do not facilitate the diffusion of niobates, dissolved from the crucible, all the way from the surface to the bulk of glass.

The presence of niobate species on the glass surface can be easily explained by the contact of melt with the niobium crucible walls, and the subsequent cooling and annealing processes conducted with the material being in the same crucible. The lack of niobate diffusion and distribution in the melt might reflect on the higher viscosity of melts corresponding to more polymerized networks, as manifested by the dominance of Q^3 groups in oxynitride-silicate glasses (e.g. Si1NNa), in contrast with phosphorous-silica glasses having mostly Q^2 groups (e.g. Si3Ca). Figure 6 compares the viscosity-temperature curves of systems similar to the three glass series of the current study. Even though the composition matches well only with 45S5 in Figure 6, the fundamental structural differences between a highly modified phosphate glass and

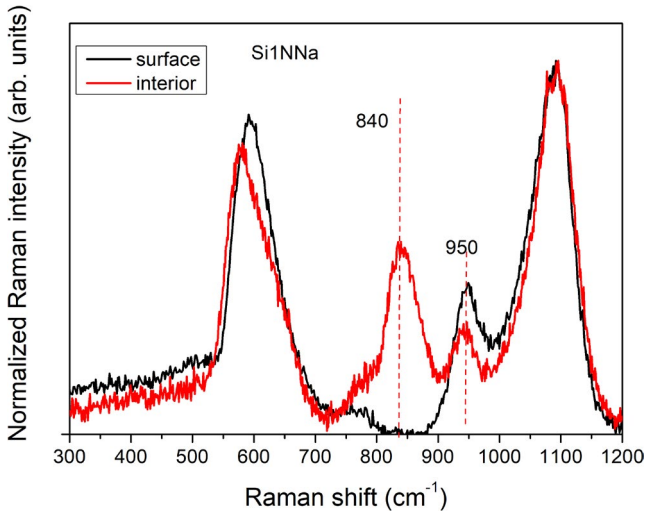

FIGURE 5 Raman spectra of glass Si1NNa measured on a fresh bulk (black) and on the surface (red) which was in contact with the niobium crucible during the melting and cooling process. Spectra were measured using the 633 nm laser line for excitation, and have been normalized on the strongest band to allow comparison (Taken from Ref. [13])

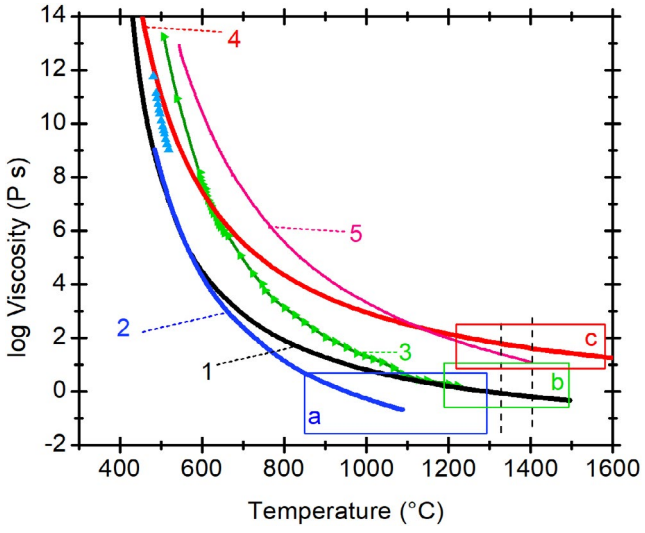

FIGURE 6 Viscosity-temperature curves of glasses similar to the three systems discussed in the current study. Phosphate glasses: (1) NSP: $10Na_2O–40SrO–50P_2O_5$ from Ehrt,[57] and (2) P45: $12Na_2O–3FeO–40Mg/CaO–45P_2O_5$ from Nusrat[58]; (3) 45S5 bio glass from Coon et al.[59]; silicate glass (4) NS: $1Na_2O–2SiO_2$ from Ehrt[57] and (5) window glass SLS from Dejneka and Kiczenski.[60] The boxes denote the experimental melting range of the three glass systems used in this study (A) P rich glass, (B) green P doped metasilicate glass and (C) BeO-silicate glass. More details in text

a polymerized silicate glass allow for a semi quantitative comparison of our glasses with the literature data. As expected, the viscosity correlates with the degree of network polymerization. Lower melt viscosities would enhance convection, mixing, and homogenous distribution of niobates in the melt, while higher viscosities would result in a lower degree of mixing and a more heterogeneous distribution of niobates close to the crucibles' walls and not throughout the bulk material.

Figure 6 includes rectangles that reflect the melting range of our three glass systems, which will be briefly discussed in the following. The BeO-silicate glasses were melted at temperatures between 1450 and 1650°C using niobium crucibles, with addition of Si_3N_4 and under nitrogen atmosphere. Solubility of niobates in the melt is the second factor to consider. Solubility is higher and viscosity is lower in melts of higher basicity, i.e. higher modifier content and lower degree of network polymerization. Thus, we have found a lack of niobate in the bulk of oxynitride-silicate glasses, while niobate is easily dissolved in the matrix of phosphorous-silicate glasses. The next glass with a more depolymerized network is the meta-silicate glass, close to the composition of bioglass 45S5, for which a lower melting temperature of around 1350°C was employed, while in the second step of preparation process, SixMg and SixCa glasses were melted at 1500–1650°C in niobium crucibles under nitrogen atmosphere and with addition of Mg or Ca metal. The last series is the phosphate glass with a composition over modified relative to the metaphosphate composition (50 mol% P_2O_5), for which the first melt is conducted at around 1000°C, and nitrification at temperatures as high as 1100 and 1600°C. It should be mentioned here that phosphate glasses are known for their high solubility for niobates as evidenced in previous studies.[51,53–55] More details about preparation parameters are included in Table 1.

As expected for glasses with high niobate solubility and low viscosities, phosphate samples show strong niobate signals in their Raman spectra as described in our previous paper,[12] noting that the 30 mol% P_2O_5 content of these glasses (as listed in Table 2) with 65 mol% modifier oxides and a small fraction of intermediate oxides leads obviously to much more depolymerized networks than the metaphosphate glass (50 mol% P_2O_5). The Raman spectra of various phosphate samples exhibit significant differences in the intensities of the niobate band at 890 cm^{-1} relative to the P–O stretching bands of the network (see Figure 7), with the analyzed niobate quantity by SEM-EDS listed in Table 2. In Table 4 and Figure 8C we tried to correlate the relative intensity of the niobate Raman signals with melting temperature and time. It can be seen that the relative intensity of the niobate band approximately scales with the niobate content

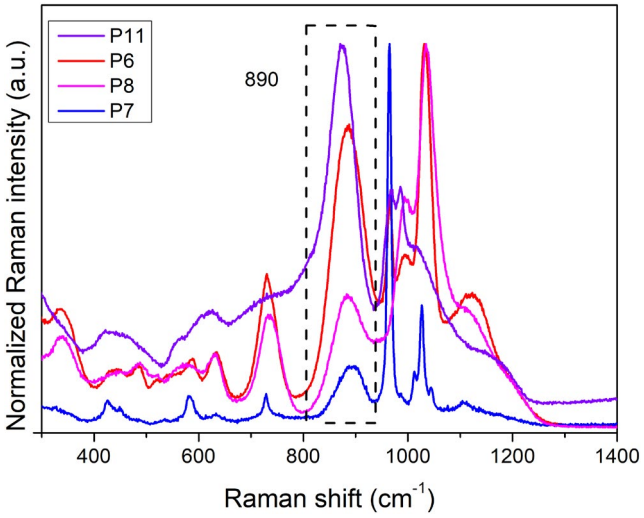

FIGURE 7 Raman spectra of samples P7, P8, P6, and P11 measured on fresh fractures of the bulk materials. Spectra have been normalized to the highest intensity band (taken from Ref. [12]). For compositions see Table 2

TABLE 4 Summary of melting parameters and correlation with the niobate content for phosphate samples. For sample compositions, see Table 2

Sample's order by Raman intensity at 890 cm^{-1}	P7<	P8<	P5<	P10<	P6<	P11=	P9
Nb content (at.%)	0.5	0.3	0.7	1.8	1.4	1.8	0.4
Maximum melting temperature (K)	1773	1673	1523	1773	1723	1823	1823
Total time of melting (min)	90	60	90	120	180	120	75
Exact batch mass (g)	1.049	1.006	1.017	1.012	1.033	1.308	0.967
Number of melts	3	1	1	2	3	2	2
Structure	Devitrified glass	Glass	Glass	Devitrified glass	Devitrified glass	Devitrified glass	Devitrified glass
Mg content (at.%)	0.4	0.7	0.3	1.3	0.4	1.6	0.9
Rel. Raman intensity	0.275	0.575	0.75	1.25	1.275	1.6	1.6

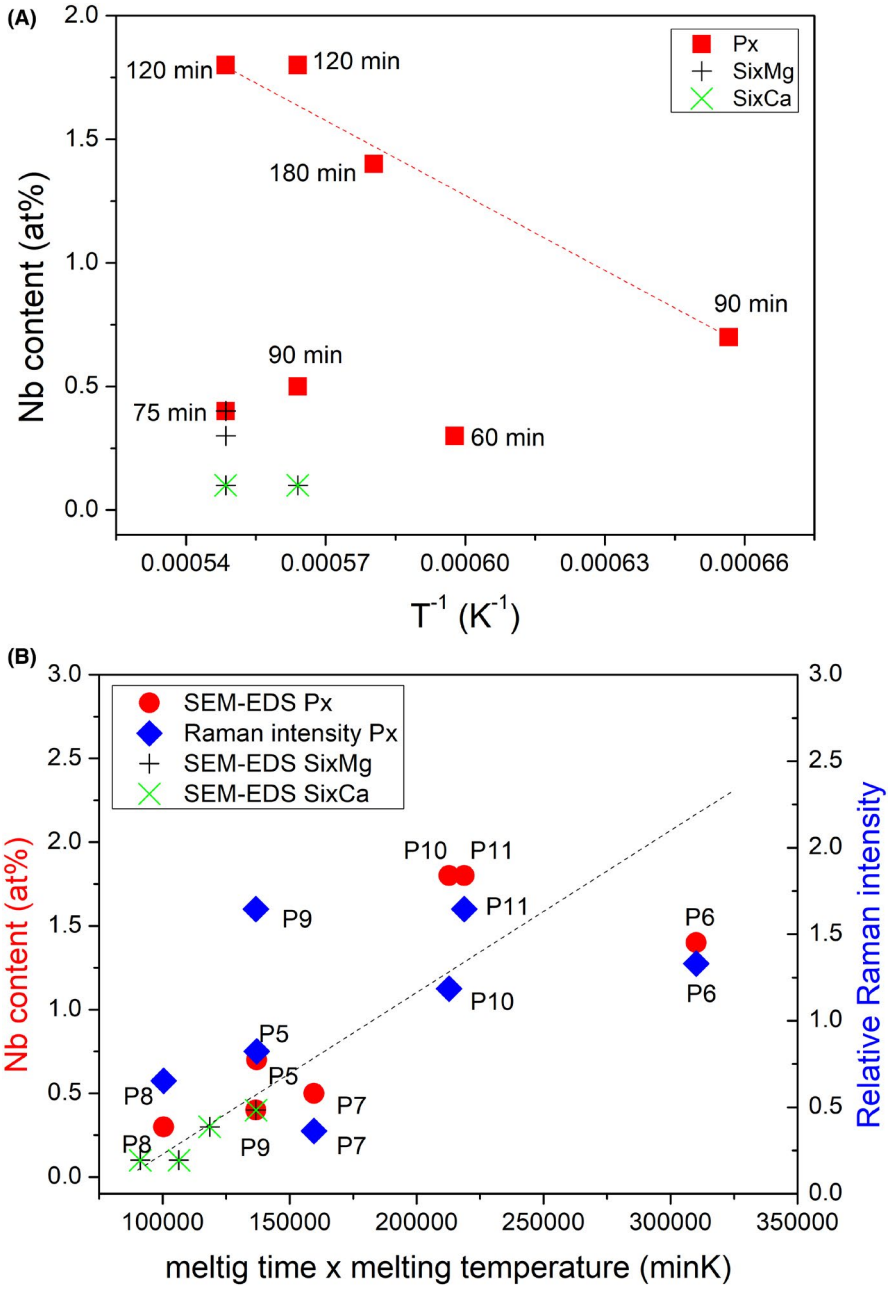

FIGURE 8 Correlation between the niobate content as obtained from SEM measurements on the processing parameters: (A) the highest melting temperature and (B) product of melting time with melting temperature, for samples in the Px, SixMg, and SixCa series, as well the Raman intensity at 890 cm^{-1} relative to the P–O stretching mode with the highest intensity for Px series (B)

as analyzed by SEM-EDS (P8,P9,P7<P5<P6<P10=P11). An exception is sample P9 with a relatively low analyzed value for niobate (0.4 at.%), but a very intense Raman band. Poor sampling statistics between bulk and surface area might be responsible for this discrepancy. Niobate data for P7 is consistent when comparing SEM and Raman values, but low for the used melting temperatures. Perhaps summing three melt cycles with heating and cooling circles overestimates the actual high temperature melting times. In Figure 8 and Figure S3, we correlated the niobium content estimated with SEM-EDS with the highest applied melting temperatures (Figure 8a) and with the melting times (Figure S3) and the combined melting temperature and time effect (Figure 8b) for series Px, SixMg, and SixCa samples. Comparing the melting parameters with the niobate content, we can assume that long melting times (longer than 90 min) play perhaps a more decisive role than the actual melting temperature in all three series of samples. Kato and Araki[56] studied the influence of temperature and glass composition on the corrosion by molten glass of zircon (34% SiO_2–65% ZrO_2) and ZrO_2 (95% ZrO_2–2.5% SiO_2–1.5% Al_2O_3) refractories. They found that the corrosion loss defined as the content of Zr/ZrO_2 that got into the glass follows the Arrhenius relation in regard to the melting temperature. Figure 8A displays analogous relationships between temperature and refractory corrosion presented as niobate content that diffused from the crucible to our samples. The Arrhenius relation is observed only for samples melted for longer time (≥90 min). However, to obtain the linear dependence the melting should be conducted during the same times.[56] One sample P7 is an exception and

instead of high melting temperature and long melting time, it was found to be low in Nb_2O_5 content as mentioned before. The effect of increase in combined temperatures and times of melting shows also a clear increase in the niobate content which penetrated into our samples.

4 | CONCLUSIONS

Remelting of a phosphorous-silicate glass (Series I), as well as pyrophosphate type glasses (Series II), in niobium crucibles results in significant niobium dissolution and incorporation of niobate species into the parent glass structure. The presence of niobates in such glasses was confirmed by Raman spectroscopy and SEM-EDS analysis. Raman spectra indicate the formation of distorted octahedral NbO_6 units, which might be connected via oxygen bridges to phosphate and silicate units. No niobium dissolution was observed in Si-rich silicate glasses (Series III), which were successfully nitrified under similar conditions. It was found that only melts of relatively high optical basicity react to a sufficient extent with the niobium crucible; the Raman niobate signal is absent in oxynitride silicate glasses ($\Lambda_{th} \approx 0.6$) and increases for phosphorous-silicate ($\Lambda_{th} \approx 0.65$) to pyrophosphate glasses ($\Lambda_{th} \approx 0.7$). The melting process parameters also effect the niobate incorporation, which increase for melting times above 90 min.

The lower basicity glass systems are characterized by more polymerized networks and, consequently, have higher viscosities in the melt. Niobate-distribution in the melts correlates with the viscosity behavior, the over modified pyrophosphate system with $\Lambda_{th} \approx 0.7$ showed niobate dissolution throughout the bulk of glass. The phosphorous-silicate glasses ($\Lambda_{th} \approx 0.65$) showed a significant niobate-gradient from the sample surface, that had been in contact with the crucible, to the inner glass where niobate levels were low, but detectable. The oxynitride Be-Si glasses ($\Lambda_{th} \approx 0.6$) showed niobate signals only at the sample surface that had been in contact with the crucible, but not signal in the sample's interior. For the strongly modified pyrophosphate glasses of high basicity, niobate dissolution was found to correlate with melting parameters, especially the product of melting temperature and melting time. Further research in this area would be helpful.

ACKNOWLEDGMENTS

NAW acknowledges the financial support from the Gdańsk University of Technology by the DEC-19/2020/IDUB/I.3.3 grant under the ARGENTUM TRIGGERING RESEARCH GRANTS - 'Excellence Initiative - Research University' program. SA and NAW acknowledge the financial support from the Crafoord Foundation (Grant No: 20160900) and Vinnova (Grant No. 2015-04809). DM thanks the Knowledge Foundation (Grant No. 68110029) for financing her stay at Linnaeus University in 2018. EIK acknowledges the project "Advanced Materials and Devices" (MIS 5002409), which is co-financed by Greece and the European Union (European Regional Development Fund).

ORCID

Natalia A. Wójcik https://orcid.org/0000-0001-7927-9187
Sharafat Ali https://orcid.org/0000-0003-1430-2862
Efstratios I. Kamitsos https://orcid.org/0000-0003-4667-2374
Doris Möncke https://orcid.org/0000-0002-4197-5520

REFERENCES

1. Tagiara NS, Palles D, Simandiras ED, Psycharis V, Kyritsis A, Kamitsos EI. Synthesis, thermal and structural properties of pure TeO_2 glass and zinc-tellurite glasses. J Non-Cryst Solids. 2017;457:116–25.
2. Palles D, Konidakis I, Varsamis CPE, Kamitsos EI. Vibrational spectroscopic and bond valence study of structure and bonding in Al_2O_3-containing AgI-$AgPO_3$ glasses. RSC Adv. 2016;6:16697–710.
3. Konidakis I, Varsamis CPE, Kamitsos EI. Effect of synthesis method on the structure and properties of $AgPO_3$-based glasses. J Non-Cryst Solids. 2011;357:2684–9.
4. Fischer B. Reduction of platinum corrosion in molten glass. Platin Met Rev. 1992;36:14–25.
5. Tagiara NS, Moayedi E, Kyritsis A, Wondraczek L, Kamitsos EI. Short-range structure, thermal and elastic properties of binary and ternary tellurite glasses. J Phys Chem B. 2019;123:7905–18.
6. Wójcik NA, Tagiara NS, Ali S, Górnicka K, Segawa H, Klimczuk T, et al. Structure and magnetic properties of BeO-Fe_2O_3-Al_2O_3-TeO_2 glass-ceramic composites. J Eur Ceram Soc. 2021;41(10):5214–22.
7. Ali S, Jonson B, Pomeroy MJ, Hampshire S. Issues associated with the development of transparent oxynitride glasses. Ceram Int. 2015;41:3345–54.
8. Sawangboon N, Nizamutdinova A, Uesbeck T, Limbach R, Meechoowas E, Tapasa K, et al. Modification of silicophosphate glass composition, structure, and properties via crucible material and melting conditions. Int J Appl Glass Sci. 2020;11:46–57.
9. Suratwala T, Campbell J, Miller P, Thorsness C, Riley M, Ehrmann P, et al. Phosphate laser glass for NIF: production status, slab selection and recent technical advances. Proc SPIE. 2004;5341.
10. Lupton DF, Merker J, Schölz F. The correct use of platinum in the XRF laboratory. X-Ray Spectrom. 1997;26:132–40.
11. Jones JR. Review of bioactive glass: from Hench to hybrids. Acta Biomater. 2013;9:4457–86.
12. Wójcik NA, Jonson B, Möncke D, Palles D, Kamitsos EI, Ghassemali E, et al. Influence of synthesis conditions on glass formation, structure and thermal properties in the Na_2O-CaO-P_2O_5 system doped with Si_3N_4 and Mg. J Non-Cryst Solids. 2018;494:66–77.
13. Wójcik NA, Jonson B, Möncke D, Kamitsos EI, Segawa H, Karczewski J, et al. The effect of nitrogen on the structure and

thermal properties of beryllium-containing Na-(Li)-Si-O-N glasses. J Non-Cryst Solids. 2019;522:119585.
14. Wójcik NA, Ali S, Mielewczyk-Gryń A, Jonson B. Two-step synthesis of niobium doped Na–Ca–(Mg)–P–Si–O glasses. J Mater Sci. 2021;56(12):7613–25.
15. Bachar A, Mercier C, Tricoteaux A, Leriche A, Follet C, Hampshire S. Bioactive oxynitride glasses: synthesis, structure and properties. J Eur Ceram Soc. 2016;36:2869–81.
16. Lenarciak A, Wójcik NA, Kupracz P, Strychalska-Nowak J, Sobczak Z, Prześniak-Welenc M, et al. Thermal, electrical, and magnetic properties of Fe_2O_3–PbO–SiO_2 glass prepared by traditional melt-quenching and twin roller fast-cooling methods. J Phys Chem Solids. 2019;135:109010.
17. Ali S, Jonson B. Compositional effects on the properties of high nitrogen content alkaline-earth silicon oxynitride glasses, AE=Mg, Ca, Sr, Ba. J Eur Ceramic Soc. 2011;31:611–8.
18. Sharafat A, Grins J, Esmaeilzadeh S. Glass-forming region in the Ca–Si–O–N system using CaH_2 as Ca source. J Eur Ceram Soc. 2008;28:2659–64.
19. Ali S, Jonson B. Glasses in the Ba-Si-O-N system. J Am Ceram Soc. 2011;94:2912–7.
20. Sharafat A, Grins J, Esmaeilzadeh S. Properties of high nitrogen content mixed alkali earth oxynitride glasses $(AE_xCa_{1-x})_{1.2(1)}SiO_{1.9(1)}N_{0.86(6)}$, AE=Mg, Sr, Ba. J Non-Cryst Solids. 2009;355:1259–63.
21. MatĚJ J, Langrova A. Reaction products and corrosion of molybdenum electrode in glass melt containing antimony oxides and sodium sulfate. Ceram Silik. 2012;56:280–5.
22. Yamamoto M, Sakai K, Akagi R, Sakai M, Yamashita H, Maekawa T. Electrochemical corrosion of molybdenum electrodes in an aluminosilicate glass melt containing antimony. J Ceramic Soc Jpn. 2004;112:179–83.
23. Wójcik NA, Ali S, Möncke D, Tagiara NS, Kamitsos EI, Segawa H, et al. The influence of Be addition on the structure and thermal properties of alkali-silicate glasses. J Non-Cryst Solids. 2019;521:119532.
24. Möncke D, Kamitsos EI, Herrmann A, Ehrt D, Friedrich M. Bonding and ion-ion interactions of Mn^{2+} ions in fluoride-phosphate and boro-silicate glasses probed by EPR and fluorescence spectroscopy. J Non-Cryst Solids. 2011;357:2542–51.
25. Duffy JA, Ingram MD. Establishment of an optical scale for Lewis basicity in inorganic oxyacids, molten salts, and glasses. J Am Chem Soc. 1971;93:6448–54.
26. Duffy JA. A review of optical basicity and its applications to oxidic systems. Geochim Cosmochim Acta. 1993;57:3961–70.
27. Duffy JA. Oxidic glasses as hosts for migrating metal ions. J Solid State Electrochem. 2011;15:87–93.
28. Dimitrov V, Komatsu T. An interpretation of optical properties of oxides and oxide glasses in terms of the electronic ion polarizability and average single bond strength. J Univ Chem Tech Metallurgy. 2010;45:219–50.
29. Rodriguez CP, McCloy JS, Schweiger MJ, Crum JV, Winschell A. Optical basicity and nepheline crystallization in high alumina glasses. Pacific Northwest National Laboratory Pacific Northwest National Laboratory; 2011.
30. Möncke D, Ali S, Jonson B, Kamitsos EI. Anion polarizabilities in oxynitride glasses. Establishing a common optical basicity scale. Phys Chem Chem Phys. 2020;22:9543–60.
31. Furukawa T, Fox KE, White WB. Raman spectroscopic investigation of the structure of silicate glasses. III. Raman intensities and structural units in sodium silicate glasses. J Chem Phys. 1981;75:3226–37.
32. Kamitsos EI, Risen WM. Vibrational-spectra of single and mixed alkali pentasilicate glasses. J Non-Cryst Solids. 1984;65:333–54.
33. McMillan P. Structural studies of silicate-glasses and melts – applications and limitations of Raman-spectroscopy. Am Miner. 1984;69:622–44.
34. McMillan P. A Raman-spectroscopic study of glasses in the system CaO-MgO-SiO_2. Am Miner. 1984;69:645–59.
35. Ross NL, Mcmillan P. The Raman-spectrum of Mgsio3 Ilmenite. Am Miner. 1984;69:719–21.
36. Mysen BO. Role of Al in depolymerized, peralkaline aluminosilicate melts in the systems Li_2O-Al_2O_3-SiO_2, Na_2O-Al_2O_3-SiO_2, and K_2O-Al_2O_3-SiO_2. Am Miner. 1990;75:120–34.
37. Zotov N. Effects of composition on the vibrational properties of sodium silicate glasses. J Non-Cryst Solids. 2001;287:231–6.
38. Malfait WJ, Zakaznova-Herzog VP, Halter WE. Amorphous materials: properties, structure, and durability†: quantitative Raman spectroscopy: speciation of Na-silicate glasses and melts. Am Miner. 2008;93:1505–18.
39. Quaranta A, Rahman A, Mariotto G, Maurizio C, Trave E, Gonella F, et al. Spectroscopic investigation of structural rearrangements in silver ion-exchanged silicate glasses. J Phys Chem C. 2012;116:3757–64.
40. O'Shaughnessy C, Henderson GS, Nesbitt HW, Bancroft GM, Neuville DR. The influence of modifier cations on the Raman stretching modes of Qn species in alkali silicate glasses. J Am Ceram Soc. 2020;103:3991–4001.
41. McMillan P, Piriou B, Navrotsky A. A Raman-spectroscopic study of glasses along the joins silica-calcium aluminate, silica-sodium aluminate, and silica-potassium aluminate. Geochim Cosmochim Acta. 1982;46:2021–37.
42. Lau J, Mcmillan PW. Interaction of sodium with simple glasses. 2. Na_2O-SiO_2 and Na_2O-Al_2O_3-SiO_2. J Mater Sci. 1984;19:881–9.
43. Kamitsos EI, Kapoutsis JA, Jain H, Hsieh CH. Vibrational study of the role of trivalent ions in sodium trisilicate glass. J Non-Cryst Solids. 1994;171:31–45.
44. Stavrou E, Palles D, Kamitsos EI, Lipovskii A, Tagantsev D, Svirko Y, et al. Vibrational study of thermally ion-exchanged sodium aluminoborosilicate glasses. J Non-Cryst Solids. 2014;401:232–6.
45. Le Losq C, Neuville DR, Florian P, Henderson GS, Massiot D. The role of Al^{3+} on rheology and structural changes in sodium silicate and aluminosilicate glasses and melts. Geochim Cosmochim Acta. 2014;126:495–517.
46. Osipov A, Osipova L, Zainullina R. Raman spectroscopy and statistical analysis of the silicate species and group connectivity in cesium silicate glass forming system. International Journal of Spectroscopy. 2015;2015:1–15.
47. Velli LL, Varsamis CPE, Kamitsos EI, Möncke D, Ehrt D. Structural investigation of metaphosphate glasses. Phys Chem Glasses. 2005;46:178–81.
48. Möncke D, Ehrt R, Palles D, Efthimiopoulos I, Kamitsos EI, Johannes M. A multi technique study of a new lithium disilicate glass-ceramic spray-coated on ZrO_2 substrate for dental restoration. Biomed Glas. 2017;3:41–55.
49. Sene FF, Martinelli JR, Gomes L. Synthesis and characterization of niobium phosphate glasses containing barium and potassium. J Non-Cryst Solids. 2004;348:30–7.

50. Cardinal T, Fargin E, Le Flem G, Leboiteux S. Correlations between structural properties of Nb_2O_5-$NaPO_3$-$Na_2B_4O_7$ glasses and non-linear optical activities. J Non-Cryst Solids. 1997;222:228–34.
51. Petit L, Cardinal T, Videau JJ, Durand E, Canioni L, Martines M, et al. Effect of niobium oxide introduction on erbium luminescence in borophosphate glasses. Opt Mater. 2006;28:172–80.
52. Dimitrov V, Komatsu T. Electronic ion polarizability, optical basicity and metal (or nonmetal) binding energy of simple oxides. J Ceram Soc Jpn. 1999;107:879–86.
53. Bih L, Azrour M, Manoun B, Graça MPF, Valente MA. Raman spectroscopy, X-ray, SEM, and DTA analysis of alkali-phosphate glasses containing WO_3 and Nb_2O_5. J Spectrosc. 2013;2013:1–10.
54. de Andrade JS, Pinheiro AG, Vasconcelos IF, Sasaki JM, de Paiva JAC, Valente MA, et al. Raman and infrared spectra of $KNbO_3$ in niobate glass-ceramics. J Phys-Condens Mat. 1999;11:4451–60.
55. Koudelka L, Kalenda P, Mošner P, Montagne L, Revel B. Structure–property relationships in barium borophosphate glasses modified with niobium oxide. J Non-Cryst Solids. 2016;437:64–71.
56. Kato K, Araki N. The corrosion of zircon and zirconia refractories by molten glasses. J Non-Cryst Solids. 1986;80:681–7.
57. Ehrt D. REVIEW Phosphate and fluoride-phosphate optical glasses - properties, structure and applications. Phys Chem Glasses - Eur J Glass Sci Technol B. 2015;56:217–34.
58. Sharmin N, Rudd CD, Parsons AJ, Ahmed I. Structure, viscosity and fibre drawing properties of phosphate-based glasses: effect of boron and iron oxide addition. J Mater Sci. 2016;51:7523–35.
59. Coon E, Whittier AM, Abel BM, Stapleton EL, Miller R, Fu Q. Viscosity and crystallization of bioactive glasses from 45S5 to 13–93. Int J Appl Glass Sci. 2021;12:65–77.
60. Dejneka M, Kiczenski TJ. Display glass. In: Musgraves JD, Hu J, Calvez L, editors. Springer handbook of glass. Springer International Publishing; 2019. p. 1521–53.

SUPPORTING INFORMATION

Additional supporting information may be found online in the Supporting Information section.

How to cite this article: Wójcik NA, Ali S, Kamitsos EI, Möncke D. Niobate in silicate and phosphate glasses: Effect of glass basicity on crucible dissolution. Int J Appl Glass Sci. 2021;00: 1–14. https://doi.org/10.1111/ijag.16505